AEDC-TR-92-2

a.2

Emission Tomography of Sodium in a Hydrogen-Air Flame

W. J. Phillips and R. Y. Walker
Sverdrup Technology, Inc., AEDC Group

July 1992

Final Report for Period October 1990 through September 1991

Approved for public release; distribution is unlimited.

ARNOLD ENGINEERING DEVELOPMENT CENTER
ARNOLD AIR FORCE BASE, TENNESSEE
AIR FORCE MATERIEL COMMAND
UNITED STATES AIR FORCE

NOTICES

When U. S. Government drawings, specifications, or other data are used for any purpose other than a definitely related Government procurement operation, the Government thereby incurs no responsibility nor any obligation whatsoever, and the fact that the Government may have formulated, furnished, or in any way supplied the said drawings, specifications, or other data, is not to be regarded by implication or otherwise, or in any manner licensing the holder or any other person or corporation, or conveying any rights or permission to manufacture, use, or sell any patented invention that may in any way be related thereto.

Qualified users may obtain copies of this report from the Defense Technical Information Center.

References to named commercial products in this report are not to be considered in any sense as an endorsement of the product by the United States Air Force or the Government.

This report has been reviewed by the Office of Public Affairs (PA) and is releasable to the National Technical Information Service (NTIS). At NTIS, it will be available to the general public, including foreign nations.

APPROVAL STATEMENT

This report has been reviewed and approved.

HAMILTON A. QUANT, 1st Lt, USAF
Directorate of Technology
Deputy for Operations

Approved for publication:

FOR THE COMMANDER

KEITH L. KUSHMAN
Director of Technology
Deputy for Operations

REPORT DOCUMENTATION PAGE

Form Approved
OMB No. 0704-0188

1. AGENCY USE ONLY (Leave blank)	2. REPORT DATE	3. REPORT TYPE AND DATES COVERED
	July 1992	Final - October 1990 - September 1991

4 TITLE AND SUBTITLE

Emission Tomography of Sodium in a Hydrogen-Air Flame

5 FUNDING NUMBERS

PN - DD22EW

6 AUTHOR(S)

Phillips, W. J. and Walker, R. Y.
Sverdrup Technology, Inc., AEDC Group

7 PERFORMING ORGANIZATION NAME(S) AND ADDRESS(ES)

Arnold Engineering Development Center/DOPT
Air Force Materiel Command
Arnold Air Force Base, TN 37389-5000

8 PERFORMING ORGANIZATION REPORT NUMBER

AEDC-TR-92-2

9. SPONSORING/MONITORING AGENCY NAMES(S) AND ADDRESS(ES)

Arnold Engineering Development Center/DO
Air Force Materiel Command
Arnold Air Force Base, TN 37389-5000

10. SPONSORING/MONITORING AGENCY REPORT NUMBER

11 SUPPLEMENTARY NOTES

Available in Defense Technical Information Center (DTIC).

12a DISTRIBUTION/AVAILABILITY STATEMENT

Approved for public release; distribution is unlimited.

12b DISTRIBUTION CODE

13 ABSTRACT (Maximum 200 words)

An investigation into the use of emission computed tomography for gas diagnostics is presented. The radiative transfer equations necessary for the determination of temperature and number density from emission data are examined. Assumptions required to cast the radiative transform equations in a form amenable for use in emission computed tomography are discussed. The Donner computed tomography algorithms are utilized to perform reconstructions of sodium 589-nm spectral line emissions from a hydrogen-air flame utilizing a square, flat flame burner.

14. SUBJECT TERMS	15. NUMBER OF PAGES
computed tomography plume diagnostics flame spectroscopy	34
	16 PRICE CODE

17 SECURITY CLASSIFICATION OF REPORT	18 SECURITY CLASSIFICATION OF THIS PAGE	19 SECURITY CLASSIFICATION OF ABSTRACT	20 LIMITATION OF ABSTRACT
UNCLASSIFIED	UNCLASSIFIED	UNCLASSIFIED	SAME AS REPORT

PREFACE

The work reported herein was conducted by the Arnold Engineering Development Center (AEDC). The results of the test were obtained by Sverdrup Technology, Inc., AEDC Group, operating contractor for the propulsion test facilities at AEDC, AFMC, Arnold Air Force Base, Tennessee, under project DD23EW. The Air Force project manager during the period covered was Capt. G. G. Nordstrom, AF/DOTR. The current Air Force project manager is 1st Lt H. A. Quant. The manuscript was submitted for publication on May 22, 1992.

CONTENTS

APPENDIX

ILLUSTRATIONS

1.0 INTRODUCTION

Computed tomography (CT) has exhibited great potential for the determination of temperature and/or specie concentration in nonaxisymmetric gas flows (Refs. 1-4). With the advent of vectoring nozzles in turbine engines and the use of multiple rocket engine nozzle combinations, a technique for determining the spatial profiles of static temperature and/or specie concentration has become important. These properties are required for code validation, heat load calculations, and signature studies. Point property measurement techniques such as laser-induced fluorescence also show promise for application to gas diagnostics (Refs. 5-8). Point property techniques are advantageous since they do not require the determination of point properties indirectly from line-of-sight measurements. However, the complexity of the equipment needed for point property techniques such as laser-induced fluorescence is far greater than that required for emission tomography. Likewise, absorption tomography also requires a substantial investment in equipment. Both these techniques require expensive and complicated tunable laser sources and their associated beam delivery systems. Computed emission tomography, on the other hand, can be applied with measurement technologies presently available such as low-light-level cameras or spatially scanning bandpass-filtered radiometers.

Presented here is a summary of an investigation into the applicability of emission tomography for gas diagnostics. The goal of this study was to determine if existing computed tomography algorithms could be employed to reconstruct emission cross-sectional profiles from emission data on high-temperature gases, and whether these data could be utilized to yield temperature and/or specie partial pressure profiles.

2.0 COMPUTED TOMOGRAPHY

Computed tomography, in a general sense, is a mathematical technique for computing a point property from line-of-sight integrals of the same property. Consider Fig. 1, in which the line integral of the property c is determined for several different paths denoted by the angles Θ and α. The path integrals of c, denoted $c(\Theta, \alpha)$ are given by

$$c(\Theta,\alpha) = \int_{P(\Theta,\alpha)} c(x,y)dS \tag{1}$$

where $P(\Theta, \alpha)$ is the path determined by the angles Θ and α. These values serve as the input to a tomographic reconstruction algorithm which would generate point properties of c, i.e., $c = c(x,y)$. Therefore, tomography can be thought of as the reverse process of Eq. (1) in which $c(x,y)$ is found from $c(\Theta, \alpha)$. No *a priori* knowledge of the function $c(x,y)$ is required.

The most readily accessible set of tomographic reconstruction algorithms is the Donner algorithms available from the Donner laboratory of Lawrence Berkeley Laboratory (Ref. 9). Although these algorithms were written primarily for the medical community, they have been employed in other areas such as nondestructive testing. The theory of tomographic reconstruction is not presented here, but there are various numerical approaches to performing Radon transforms such as direct algebraic inversion techniques, two-dimensional Fourier transform analysis, and iterative techniques. The Donner computer code contains all the major reconstruction techniques, as well as means to handle several different source and/or detector geometries.

3.0 RADIATIVE TRANSFER

An optical gas diagnostic technique employing CT must satisfy two basic requirements. One requirement is that the reconstructed quantity must be a function of temperature, number density, or other desired flow parameters. The other requirement, which is essential for the application of tomography, is that from the measured quantity, a line-of-sight integral of the reconstructed quantity must be obtained which will serve as input for a tomographic reconstruction. For example, consider a measurement of transmittance. The transmittance is not a line-of-sight integral of some quantity. However, a line-of-sight (LOS) integral of the absorption coefficient can be extracted from the transmittance measurements utilizing Beer's law:

$$\tau(\Theta,\alpha) = e^{-K(\Theta,\alpha)} = e^{-\int_{P(\Theta,\alpha)} k_a(x,y)dS} \tag{2}$$

where τ is the transmittance, $k_a(x,y)$ is the absorption coefficient, $K(\Theta, \alpha)$ is the LOS-integrated absorption coefficient, and $P(\Theta,\alpha)$ represents the integration path as shown in Fig. 1. The integrated absorption coefficient is easily calculated from the measured transmittance:

$$K(\Theta,\alpha) = \int_{P(\Theta,\alpha)} k_a(x,y)dS = -\ell n\tau(\Theta,\alpha) \tag{3}$$

Since this is an LOS integral, it is applicable to tomographic reconstruction, and since the absorption coefficient is temperature- and number density-dependent, the transmittance is a possible tomography gas diagnostic tool (Refs. 10-11). To investigate the applicability of emission measurements for tomography reconstruction, consider radiative transfer through a nonhomogeneous gas. The radiative transfer equation is given by:

$$N(\lambda) = \left[\frac{A_{if}hc10^7 f(\lambda)}{4\pi\lambda}\int_o^\ell n_i e^{\int_o^x k_a dx'} dx + N_o(\lambda)\right] e^{-\int_o^\ell k_a dx} \tag{4}$$

where the symbols are defined as follows:

A_{if}	Transition probability, sec^{-1}
c	Speed of light, $cm\text{-}sec^{-1}$
h	Planck's constant, erg-sec
n_i	Number density of emitting atoms in initial state i, cm^{-3}
λ	Wavelength of spectral line, nm
$N(\lambda)$	Emitted spectral radiance, $w/(cm^2\text{-}sr\text{-}nm)$
$N_o(\lambda)$	Incident spectral radiance, $w/(cm^2\text{-}sr\text{-}nm)$
k_a	Absorption coefficient, cm^{-1}
$f(\lambda)$	Spectral line shape function, nm^{-1}
l	LOS path length

The absorption coefficient above includes the stimulated emission term and is given by:

$$k_a = \frac{n_f \lambda^4 10^{-21} f(\lambda) A_{if}}{8\pi c} \left(1 - e^{-hc10^7/\lambda kT}\right) \tag{5}$$

where n_f is the number density of atoms in the final (lower) state and T is the temperature. Assuming the gas is in thermal equilibrium, the number density of emitting atoms in state i is distributed according to a Maxwell-Boltzmann distribution and is given by:

$$n_i = n \frac{g_i e^{-E_i hc/kT}}{Q(T)} \tag{6}$$

where the symbols are defined by:

E_i	Energy of ith state, cm^{-1}
Q(T)	Partition function
T	Temperature, K
k	Boltzmann's constant, erg K^{-1}
n	Total number density of emitting atoms, cm^{-3}
g_i	Degeneracy of i^{th} state

The spatial dependence of the spectral radiance is through the temperature and number density which are position dependent. Examination of Eq. (4) indicates that from a measurement of the emitted spectral radiance alone, one cannot determine a simple line integrable quantity. However, if it is assumed the gas is optically thin (i.e., no self absorption, $k_a = 0$) and there is no incident radiation ($N_o = 0$), Eq. (4) reduces to:

$$N(\lambda) = \frac{A_{if} hc 10^7 f(\lambda)}{4\pi\lambda} \int_o^\ell n_i dx \tag{7}$$

If one assumes that the spectral instrument response function, $g(\lambda)$, of the detecting system is wide in comparison to the spectral line width of the emitting radiation, the measured radiance is approximately given by:

$$N = \frac{A_{if} hc 10^7 g(\lambda o)}{4\pi\lambda o} \int_o^\ell n_i dx \tag{8}$$

where λ_o is the emitting spectral line position.

A comparison of Eq. (8) and Eq. (1) indicates the measured radiance has the desired LOS integrability for use as input to computed tomography. Note the reconstructed quantity is a multiplicative factor of the number density of the radiating atoms in the initial quantum state. Equation (6) expresses this as the total number density of the emitting atoms and the temperature. Therefore, it is possible to determine the number density of the radiating species from the reconstructed state specific number densities, provided the spatial profile of the temperature is known.

Measurement of two radiances originating from two different spectral lines of the same species could be utilized to simultaneously determine both number density and temperature under certain instances. Consider two spectral lines, λ_o and λ_o', from the same specie originating from two different energy levels, E_i and E_i'. Reconstruction of the measured radiances would yield the following reconstructed quantities:

$$c(x,y) = \frac{A_{if} hc 10^7 g(\lambda o)}{4\pi\lambda o} n_i(x,y) \tag{9}$$

and

$$c'(x,y) = \frac{A_{if}' hc 10^7 g(\lambda o')}{4\pi\lambda o'} n_i'(x,y) \tag{10}$$

Taking the ratio of the two reconstructed quantities yields:

$$\frac{c(x,y)}{c'(x,y)} = \frac{A_{if} g(\lambda o)\lambda o'}{A_{if}' g(\lambda o')\lambda o} \frac{n_i(x,y)}{n'_i(x,y)} \tag{11}$$

which, with the help of Eq. (6), can be rewritten as

$$\frac{c(x,y)}{c'(x,y)} = \frac{A_{if} g(\lambda o)\lambda o' g_i}{A_{if}' g(\lambda o')\lambda o g'_i} e^{-(E_i - E_i')/kT} \tag{12}$$

Values for the Einstein spontaneous emission coefficient, A, degeneracy, and wavelengths can be found in the literature, and the instrument function can be established from the

instrument calibration (Ref.12). Once these parameters are established, the temperature equation [Eq. (12)] above can be solved for temperature:

$$T(x,y) = \frac{E_i - E_i'}{k\ln\left[\frac{c(x,y)\lambda_o A_{if}' g(\lambda_o') g_i}{c'(x,y)\lambda_o A_{if} g(\lambda_o) g_i'}\right]} \tag{13}$$

Once the temperature is known at each spatial location, Eqs. (6) and (9) (or 10) can be employed to determine the number density:

$$n(x,y) = \frac{c(x,y)4\pi\lambda_o Q(T)}{A_{if} hc 10^7 g(\lambda_o) g_i e^{-E_i/kT}} \tag{14}$$

4.0 EXPERIMENTAL APPROACH

The sodium doublet at 589 and 589.5 nm was chosen for the emission tomography measurements. This doublet appears as a single spectral line at moderate resolution and has been observed to occur in varying degrees in most engine plumes. The radiation from sodium at this wavelength and from the potassium doublet at 766.5 and 769.9 nm is consistently observed in the hydrogen-oxygen space shuttle main engine (SSME) plume. This flame cannot be duplicated in the lab, but a hydrogen-air flame can be created utilizing a small-scale burner. Since both sodium and potassium are excellent radiators, the number density required to yield the observed radiation levels in the SSME is extremely low. An analysis of SSME signature data indicated that the radiance due to sodium and potassium was approximately equal at the nozzle exit plane; however, the concentration required to yield the observed radiation level was determined to be 0.87 and 0.06 ppb, respectively (Refs 13). Recent measurements on MMH-N_2O_4 (monomethylhydrazine) and UDMH-N_2O_4 (unsymmetrical dimethylhydrazine) propellant engines have indicated that they also possess sodium emissions in their plumes.

The 589- to 589.5-nm doublet is the only spectral feature of sodium or potassium that is consistently and easily observed at moderate spectral resolution in exhaust plumes. This is unfortunate, since it precludes the use of emission measurements from two spectrally resolved lines of the same gas to simultaneously determine both temperature [from Eq. (13)] and number density [from Eq. (14)]. Therefore, a temperature profile must be determined independently. This temperature profile can then be employed to determine the number density from the reconstructed emission coefficients by using Eq. (14).

A proof-of-principle experiment was designed around the use of a flat flame burner. The particular burner used was a 2-in.-square burner shown in Fig. 2 obtained from Research Technologies. The body of the burner consisted of a Hastalloy® honeycomb interlaced with

0.02-in.-ID hypodermic tubes shown in Fig. 3. The hydrogen was delivered by the hypodermic tubes, and the oxidizer by the voids in the honeycomb. Hydrogen and air flow rates were measured using Edwards-Datametrics 50 and 100 slpm (standard liters per minute) full-scale digital flow meters, respectively.

4.1 SODIUM LASER ABSORPTION MEASUREMENTS

The first measurements on the burner system were sodium spectral absorption measurements to determine the extent of self absorption. The configuration for this experiment is shown in Fig. 4. The source utilized is an argon-ion laser-pumped tunable ring dye laser. The dye laser output was split between a laser fluorescence reference cell and the probe beam which traversed the flat flame burner approximately 0.75 in. above the burner base. The signal from the fluorescence reference cell was used to indicate when the laser had been tuned to the sodium absorption line. These measurements were conducted over a wide range of flow conditions and no measurable absorption was found. This implies that the necessary criterion for the use of emission tomography is met; that is, an optically thin medium is assumed.

4.2 TOMOGRAPHY EMISSION MEASUREMENTS

Tomographic emission data were acquired using a low-light-level camera. The camera selected was a Burle model 07985 since it is equipped with an automatic gain control (AGC) enable/disable option. This feature allows acquisition of images under varying light conditions that are indicative of the true light level. The camera was equipped with a Nikon f/4 80-200 mm zoom lens which gave an image of the burner which filled approximately 75 percent of the video frame at a source distance of 51 in. Mounted to the front of the lens was a bandpass optical filter. The transmission curve of the filter is shown in Fig. 5 from which the center wavelength and bandpass are found to be 588 and 5 nm, respectively. The output of the low-light-level camera was recorded on VHS video tape which was later played back for analysis.

To obtain images of the flame at various angles, the flat flame was mounted on a rotation-translation stage as shown in Fig. 2. This allowed the burner to be rotated through 180 deg. Figure 6 is a schematic diagram of the experimental setup, and the photograph in Fig. 2 shows the position of the camera in the upper left and its relation to the burner. All data were taken 0.75 in. above the burner face.

Processing of the video was performed on a Quantex image processor. Individual frames corresponding to the various angles were digitized. From these frames, an individual horizontal scan corresponding to a slice 0.75 in. above the burner face was taken, as illustrated in Fig.

6. These data then served as input to the tomography algorithms. Data were taken every 12 deg over 180 deg, with each slice consisting of 235 pixels. The flow rates through the burner were 16.57 slpm hydrogen and 36.47 slpm air, which yields an equivalence ratio of 1.11. Flow settings were chosen to achieve the maximum sodium emission; this was checked by observing the camera video output. Repeated operation of the burner indicated that maximum radiation in the 588-nm region was not consistent with the flow settings.

The horizontal slices of the flame image were used as input to the Donner tomographic reconstruction algorithms. The fan-beam geometry option of the Donner algorithms was selected for data reduction and the conjugate gradient technique for reconstruction. Appendix A is a listing of the main subroutine used to invoke the tomography algorithms. Figure 8 illustrates the resulting reconstructed images which can be compared to the color photograph (Fig. 7) of the H_2-air flame. Note the nonuniformity and strong emission characteristics in both the photograph and reconstructed image which appears in the periphery of the flame.

Contrary to our initial assumptions, the flame was far from uniform. This discovery poses a substantial problem from the standpoint of modeling. If the fuel-air mixture is not uniformly distributed across the burner face, then using the adiabatic flame temperature from the NASA 273 equilibrium chemistry code for the flame temperature would be in error (Ref. 14). An attempt was made to measure the flame temperature by traversing a Pt-Pt/Rh thermocouple through the flame. Figure 9 illustrates the results of the thermocouple traverses. The temperature shown in Fig. 9 is the thermocouple temperature, not the gas temperature. A difference exists between these measurements because of the convective-radiative heat-transfer losses. Two features are apparent from examination of the thermocouple data: the nonuniform distribution and the low measured temperature values. The measured temperatures are lower than the adiabatic flame temperature, 2,404 K, by approximately 1,200 K. This difference is far greater than could be explained by convective-radiative heat-transfer losses from the thermocouple which would introduce an error of approximately 100 K. An explanation can be found in examining Fig. 7. Note the radiation from the burner face (an extremely bright glow) which implies a substantial heat transfer to the burner face and, therefore, may explain the lower measured flame temperature. Nonuniformities in the flow were initially thought to be due to nonuniform distributions in the mixing of fuel and oxidizer.

To examine the nonuniformity in the fuel-air ratio, a series of mass spectrometer measurements was made across the burner face. A 1/8-in.-diam probe attached to a mass spectrometer was traversed across the burner 0.75 in. above the burner face. The hydrogen fuel was replaced by argon and the air oxidizer was replaced by N_2. Figure 10 illustrates the results of the measured argon/N_2 ratio profiles. Note that in the main center portion of the burner area, a uniform mix was obtained. Data in the periphery of the flow are less accurate due to the small concentration of Ar, where as much as a factor of two difference is seen

in the different regions of the burner. Based on the mass spectrometer profiles, particularly in the 0- to 20-mm region of the burner, the temperature nonuniformities cannot be attributable to poor mixing.

While investigating the sodium radiation, researchers discovered that the burner face temperature played an important role in the sodium emission level. Further investigation led to the discovery that placing an object such as a stainless steel tube in the flame can induce stronger sodium emission. If the tube is cooled, the sodium radiation essentially disappears; however, when allowed to reheat in the flame, a bright sodium radiation is observed. Figure 11 is a spectrum obtained by employing an optical multichannel analyzer (OMA) to view the region above the heated tube. The spectrum illustrates the presence of both sodium and potassium in the flame above the heated tube. When cooled by flowing water through the tube, the radiation from the sodium and potassium decreased in intensity until it was indistinguishable from the background noise, although, to a lesser extent, the same result was obtained from the burner itself. When the burner was operated at the highest flow rates achievable with the present system, the flame partially detached from the burner face.This decreased the heat transfer to the burner, and a marked decrease in the sodium radiation levels was measured. Conversely, lowering the overall gas flow rates raised the burner face temperature, and a substantial increase in sodium and potassium emission levels was observed. Although there is no explanation of this phenomenon at present, the mechanism responsible for sodium excitation is important. If sodium is to be used as a diagnostic tool in tomography or laser-induced fluorescence, the understanding of its excitation mechanism is important for use in gas diagnostic modeling computer codes.

5.0 SUMMARY

The radiative transfer equations for atomic spectral line radiation emanating from a hot gas were examined for applicability to tomography. Methodologies for determining temperature and/or number densities from the reconstructed quantities were derived. A proof-of-principle experiment was performed to demonstrate the applicability of emission tomography. Tomography data consisting of atomic sodium radiation from a H_2-air flame from a flat flame burner were acquired using an optically filtered low-light-level camera. The sodium radiation data were reconstructed by application of the Donner tomography algorithms. Based on visible photographs and visual examination of the flame, the reconstructed image was found to be consistent with observations. However, large nonuniformities in the flame were observed. These nonuniformities and discretions between equilibrium chemistry code results and measured thermocouple data precluded a quantification of the sodium number density or temperature from the data. Further investigation into the source of the nonuniformities suggested that a surface reaction mechanism is responsible for the excitation of sodium in the flame. At this time the exact nature of this mechanism is unclear.

6.0 RECOMMENDATION

A quantifiable flame is required to thoroughly test the applicability of tomography for diagnostics. Although it has been shown that it is possible to reconstruct emission images consistent with visual observation, a more detailed and controlled experiment is required to test the ability of emission tomography for temperature and number density determination. The sodium excitation process appears to be surface related and not quantifiable at this time. Therefore, it would be advantageous to use another specie that can be easily seeded into the fuel or oxidizer. If a seed specie can be identified which will equilibrate to the flame temperature and has sufficient emission characteristics, a more detailed experimental study would be in order. This may require the use of a higher temperature flame such as a hydrogen-oxygen flame to create sufficient excitation energies to excite the seeded specie(s). Such an experiment requires sufficient gas flow capabilities to achieve gas velocities above the burner face high enough to lift the flame front off the face of the burner and lower the heat transfer to the burner. Under these circumstances, a modeling of the flame chemistry and temperature should be sufficiently accurate to use as a control in an experiment to test temperature and/or number density diagnostics using emission tomography.

REFERENCES

1. Ray, S. and Semerjian, H. G. "Laser Tomography for Simultaneous Concentration and Temperature Measurement in Reacting Flows." AIAA-83-1553, AIAA 18th Thermophysics Conference, June 1, 1983, Montreal, Canada.

2. Carpenter, K. H. and Lazar, N. H. "NCMART: Algorithms and Computer Codes for a Modified Algebraic Spatial Reconstruction of Spectroscopic Emissivities for ELMO Bumpy Torus." Report No. ORNL/TM-6500, Oak Ridge National Labs, November 1978.

3. Hertz, H. M. and Faris, G. W. "Emission Tomography of Flame Radicals." *Optics Letters*, Vol. 13, No. 5, May 1988, p. 351.

4. Goulard, R. and Emmerman, P. J. "Absorption Diagnostics."AIAA-79-0085, AIAA 17th Aerospace Sciences Meeting, January 1979, New Orleans, LA.

5. Miles, R. B. "Resonant Doppler Velocimeter." *The Physics of Fluids*, Vol.18, No. 6, June 1975, p. 751.

6. Fairbank, W. M., Hansch, T. W., and Schawlow, A. L. "Absolute Measurement of Very Low Sodium-Vapor Densities Using Laser Resonance Fluorescence." *Journal of the Optical Society of America*, Vol. 65, No. 2, February 1975, p. 199.

7. Kaijiwara, T., et al. "Application of Two-Photon-Excited Laser-Induced Fluorescence to Atomic Hydrogen Measurements in the Edge Region of High-Temperature Plasmas." *Reviews of Scientific Instruments,* Vol. 62, No. 10, October 1991, p. 2345.

8. Westblom, U., et al. "Detection of Nitrogen Atoms in Flames Using Two-Photon Laser-Induced Fluorescence and Investigations of Photochemical Effects." *Applied Optics,* Vol. 30, No. 21, July 1991, p. 2990.

9. Huesman, R. H., et al. "Users Manual: Donner Algorithms for Reconstruction Tomography." Donner Laboratory-Lawrence Berkeley Laboratory, University of California, Berkeley, CA, October 1977.

10. Penner, S. S. *Quantitative Molecular Spectroscopy and Gas Emissivities.* Addison-Wesley Publishing Co., Inc., Reading, MA, 1959.

11. Hanson, R. K. "Combustion Gas Measurements Using Tunable Laser Absorption Spectroscopy." Proceedings of 17th Aerospace Sciences Meeting, 15-17 January 1979, New Orleans, LA.

12. Corliss, C. H. and Bozman, W. R. "Experimental Transition Probabilities for Spectral Lines of Seventy Elements." National Bureau of Standards Monograph 53, July 1962.

13. Cikanek, H. A. et al. "Space Shuttle Main Engine Plume Spectral Monitoring Preliminary Results." AIAA-87-1792, AIAA/SAE/ASME/ASEE 23rd Joint Propulsion Conference, June 1987, San Diego, CA.

14. Gordon, S. and McBride, B. J. "Computer Program for Calculation of Complex Chemical Equilibrium Compositons, Rocket Performance, Incident and Reflected Shocks, and Chapman-Jouguet Detonations." NASA Lewis Research Center, NASA SP-273, 1971.

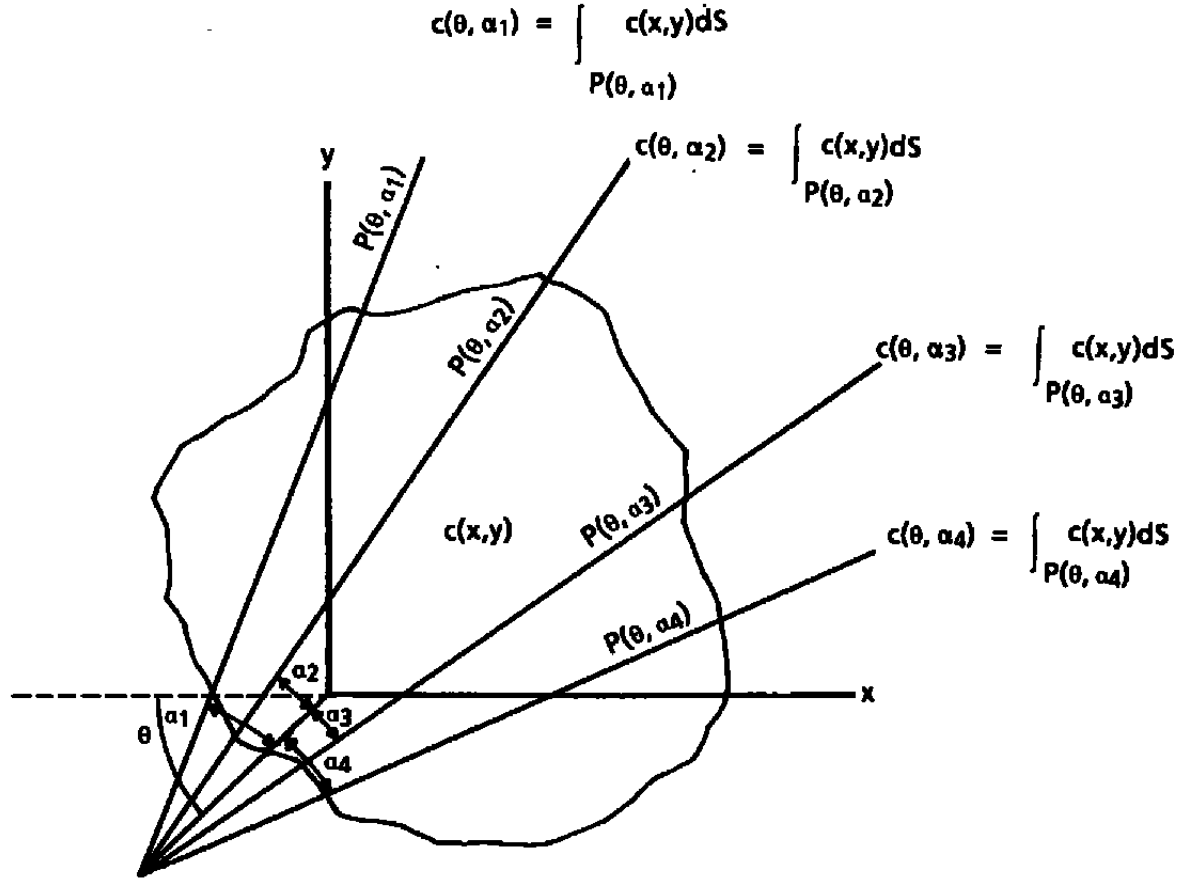

Figure 1. Geometry model describing relations of tomographic quantities.

Figure 2. Photograph of flat flame burner and tomography experimental setup.

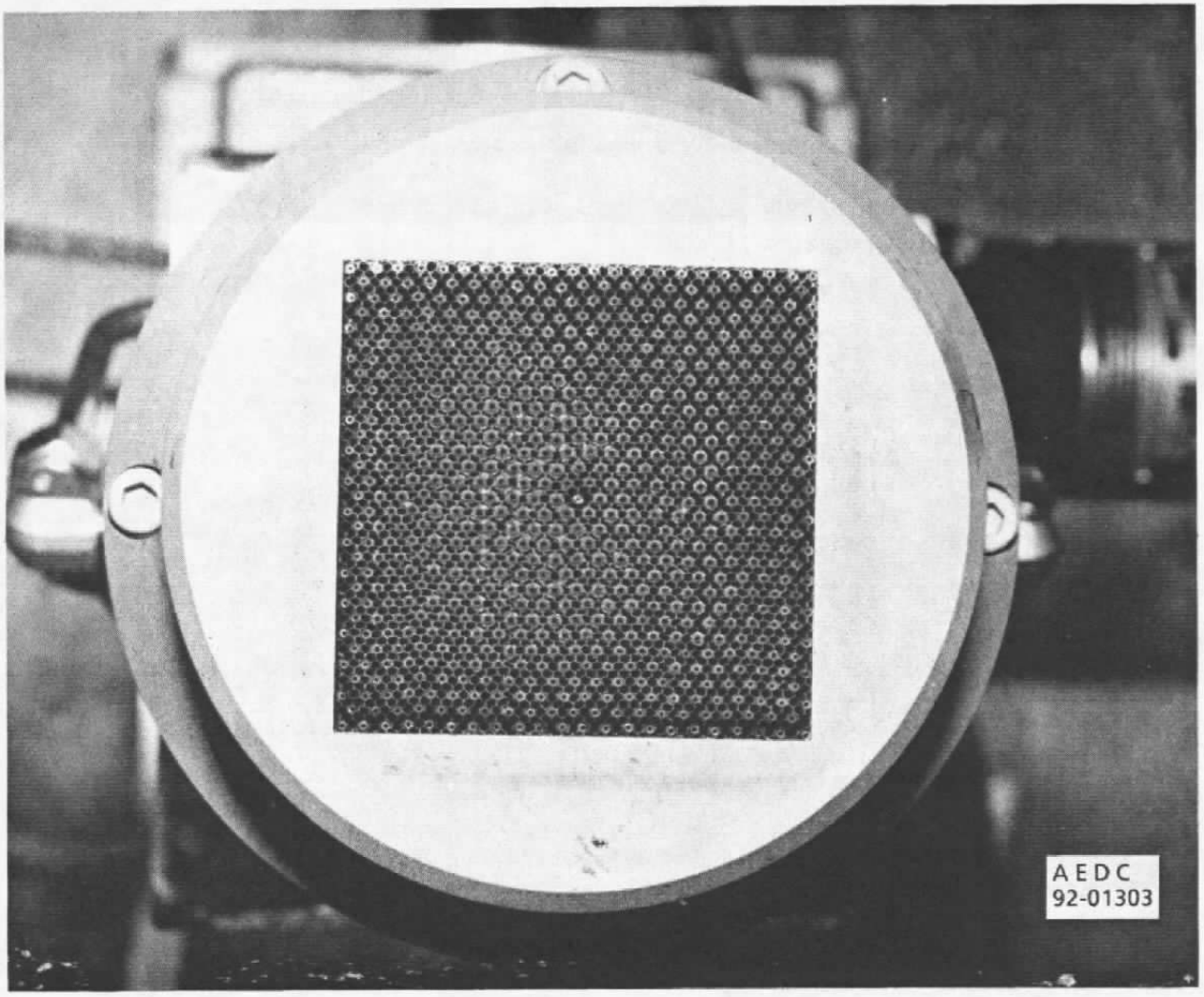

Figure 3. Photograph of flat flame burner face showing array of hypodermic tubes in Hastalloy® honeycomb.

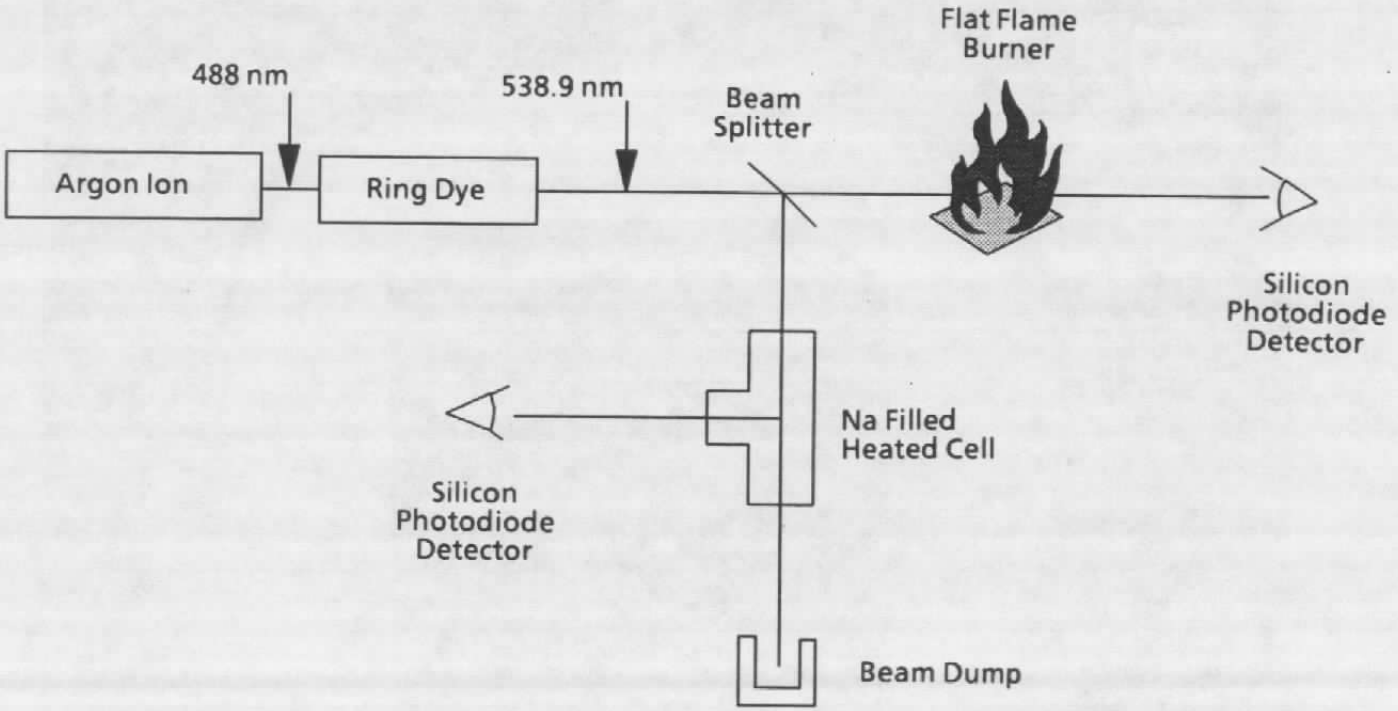

Figure 4. Sodium laser absorption experimental configuration.

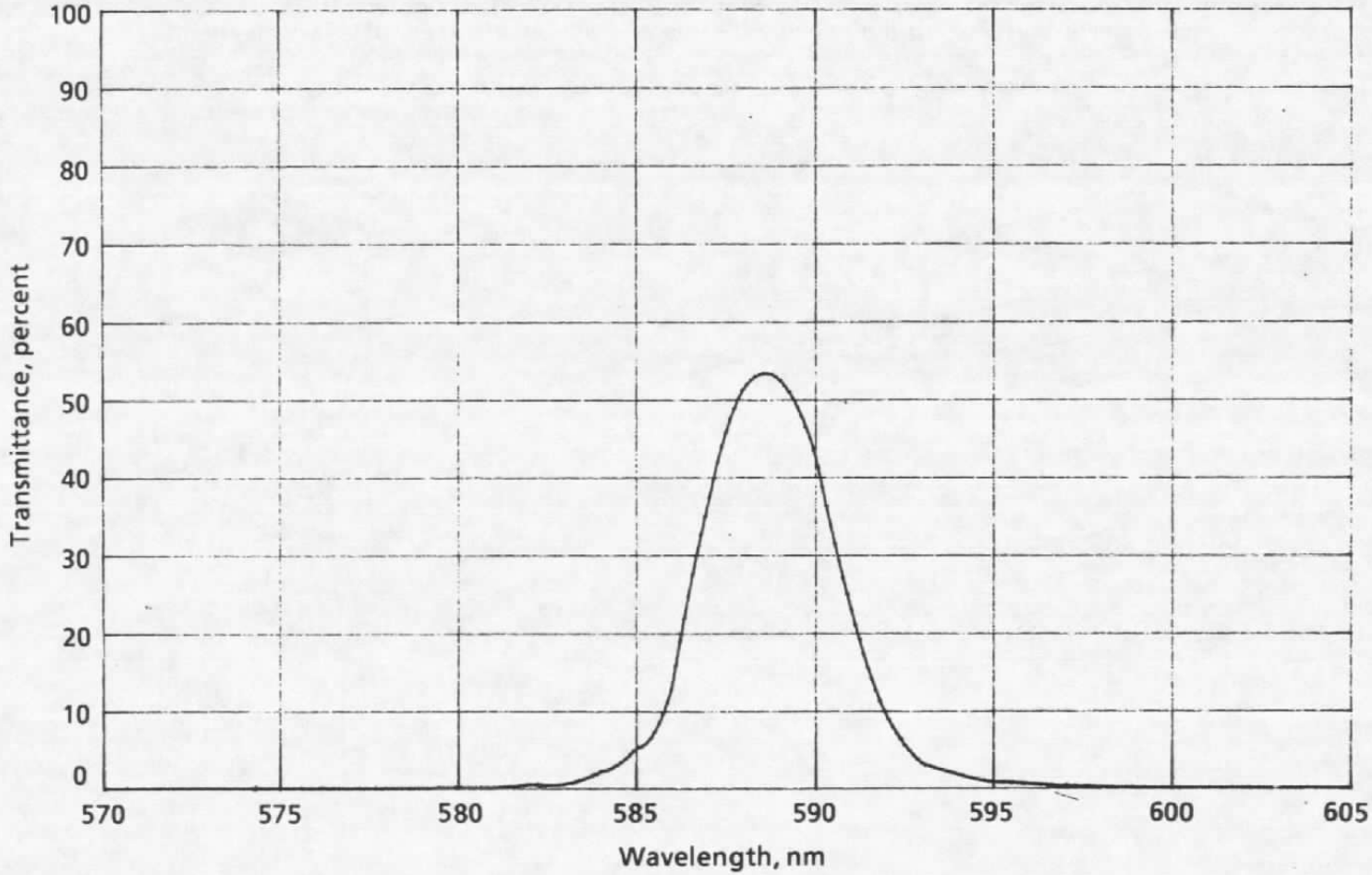

Figure 5. Sodium optical filter transmission curve.

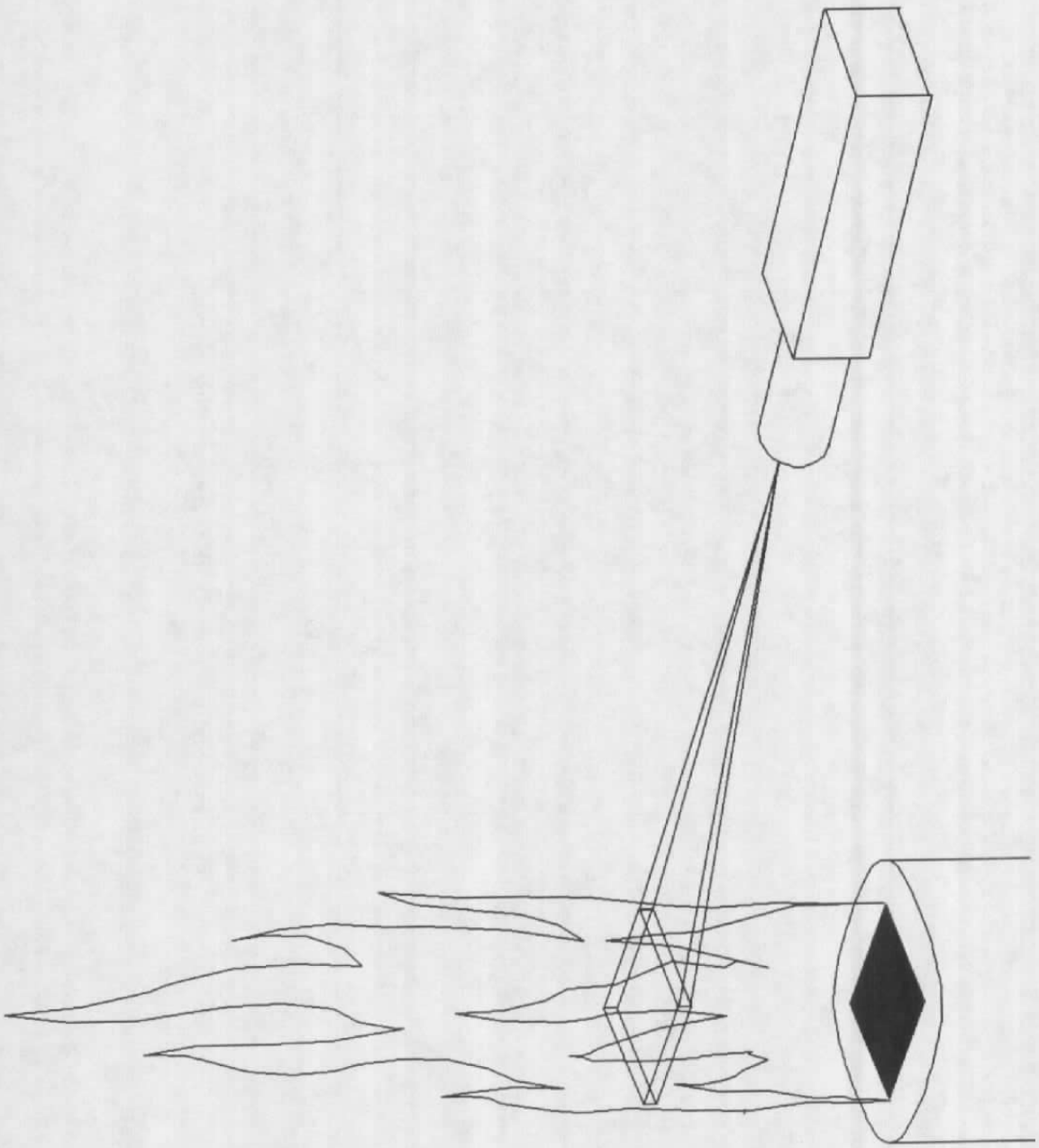

Figure 6. Schematic of tomographic emission experiment and the digitized field of view required for tomographic reconstruction.

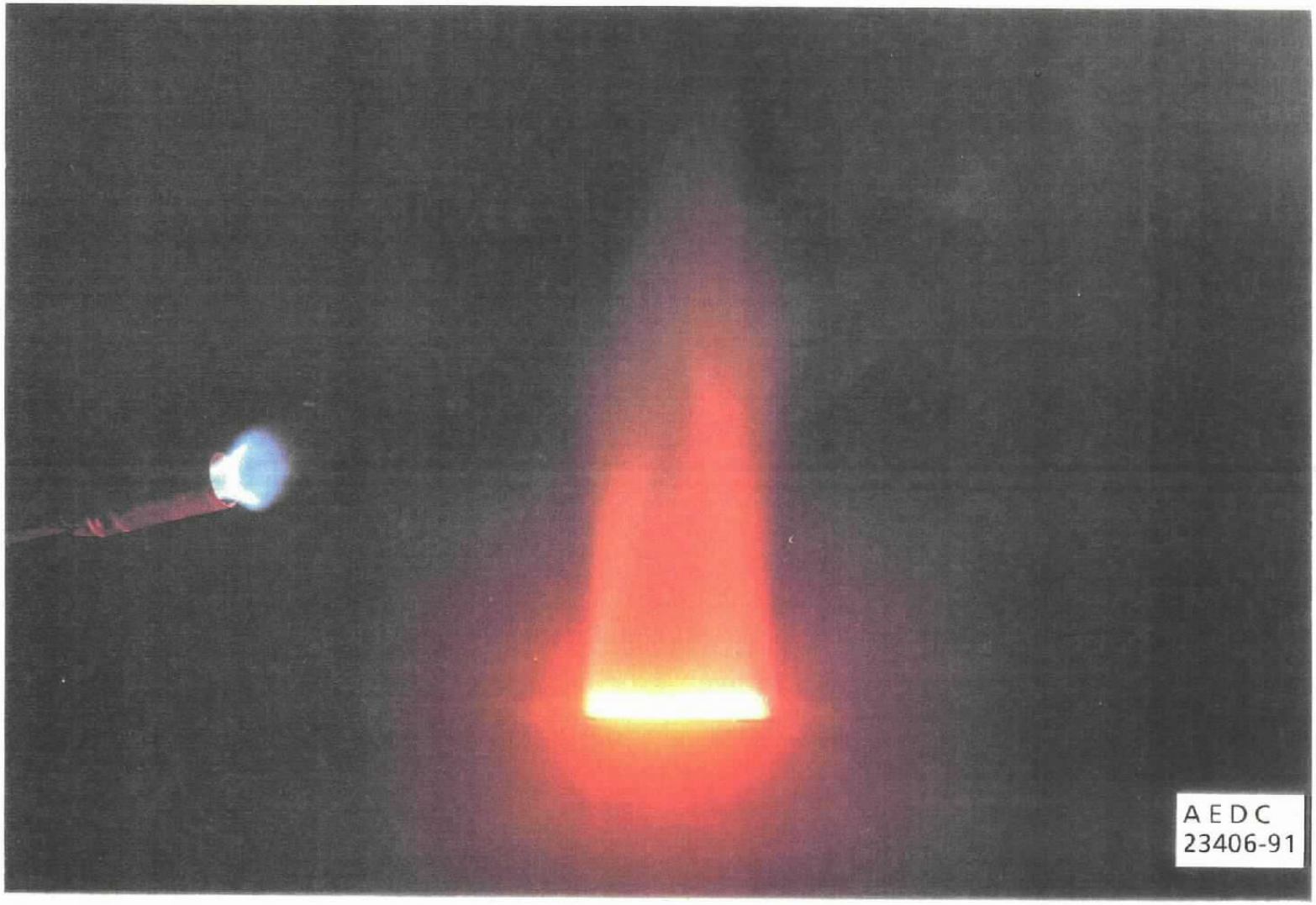

Figure 7. Non-filtered photograph of H_2-air flame on flat flame burner.

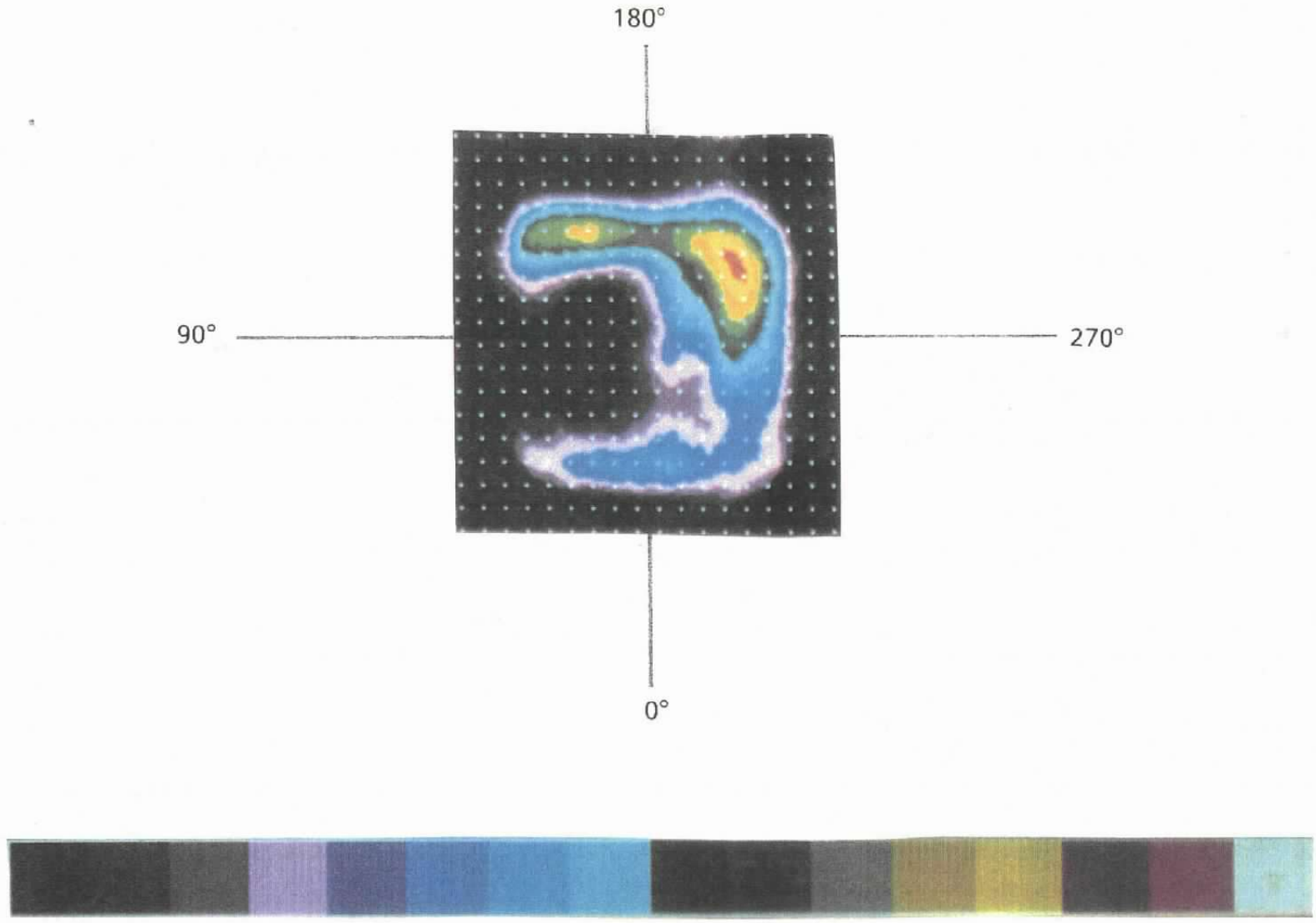

Figure 8. Reconstructed sodium emission profile from H_2O-air flat flame burner utilizing bandpass-filtered camera data.

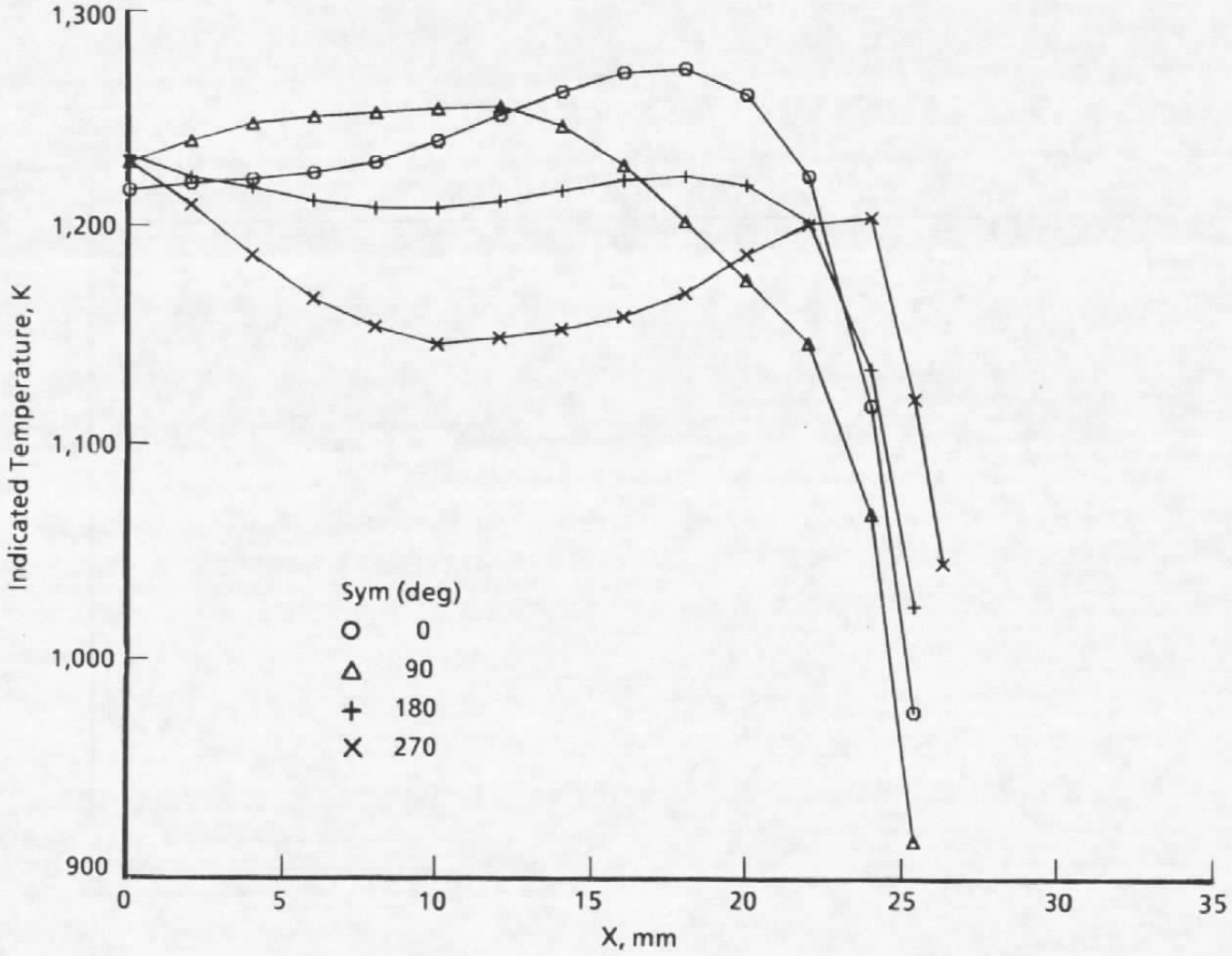

Figure 9. Indicated temperature spatial scans 0.75 in. above the H_2-air flat flame burner.

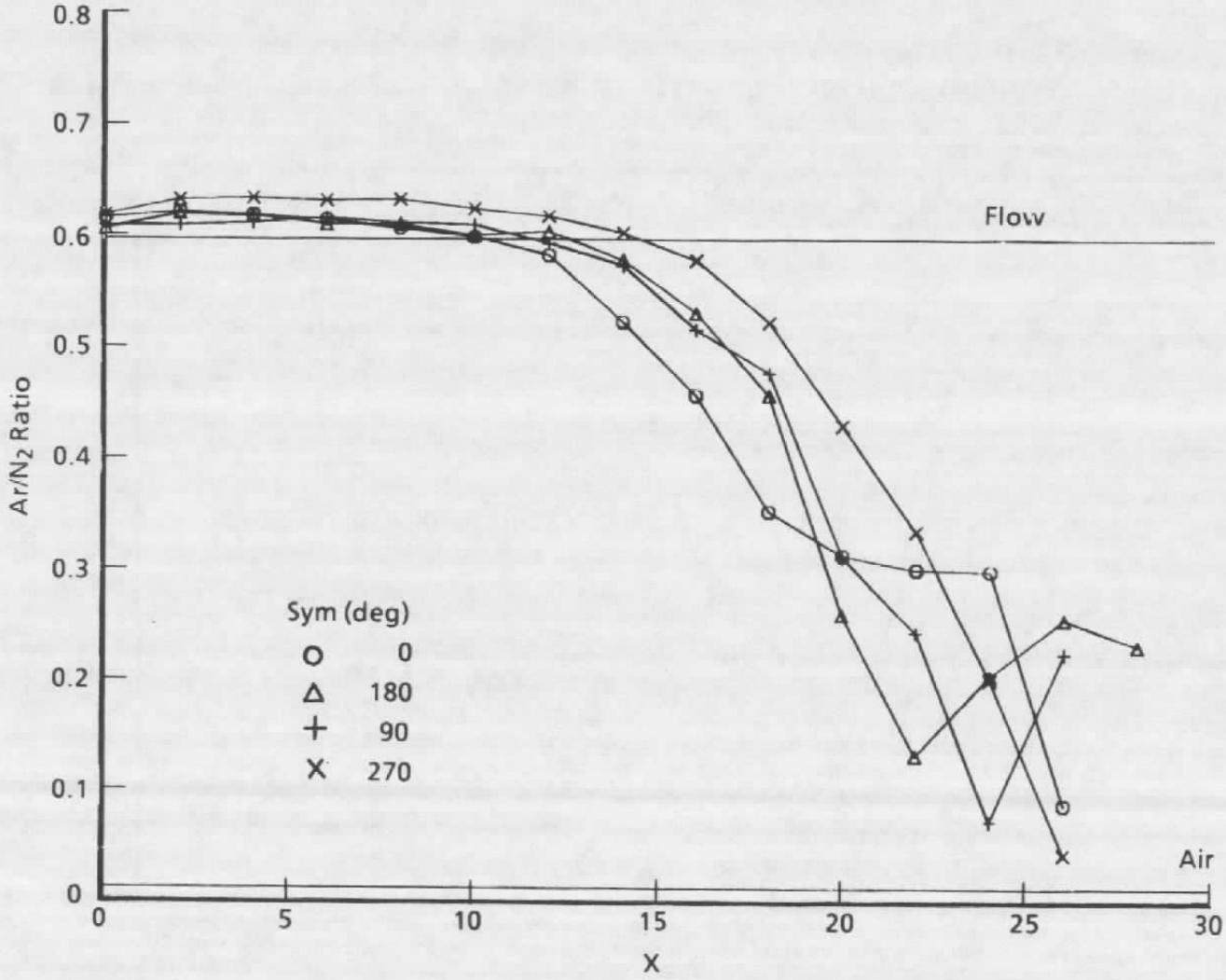

Figure 10. Ratio of abundance of air to N_2 above flat flame burner.

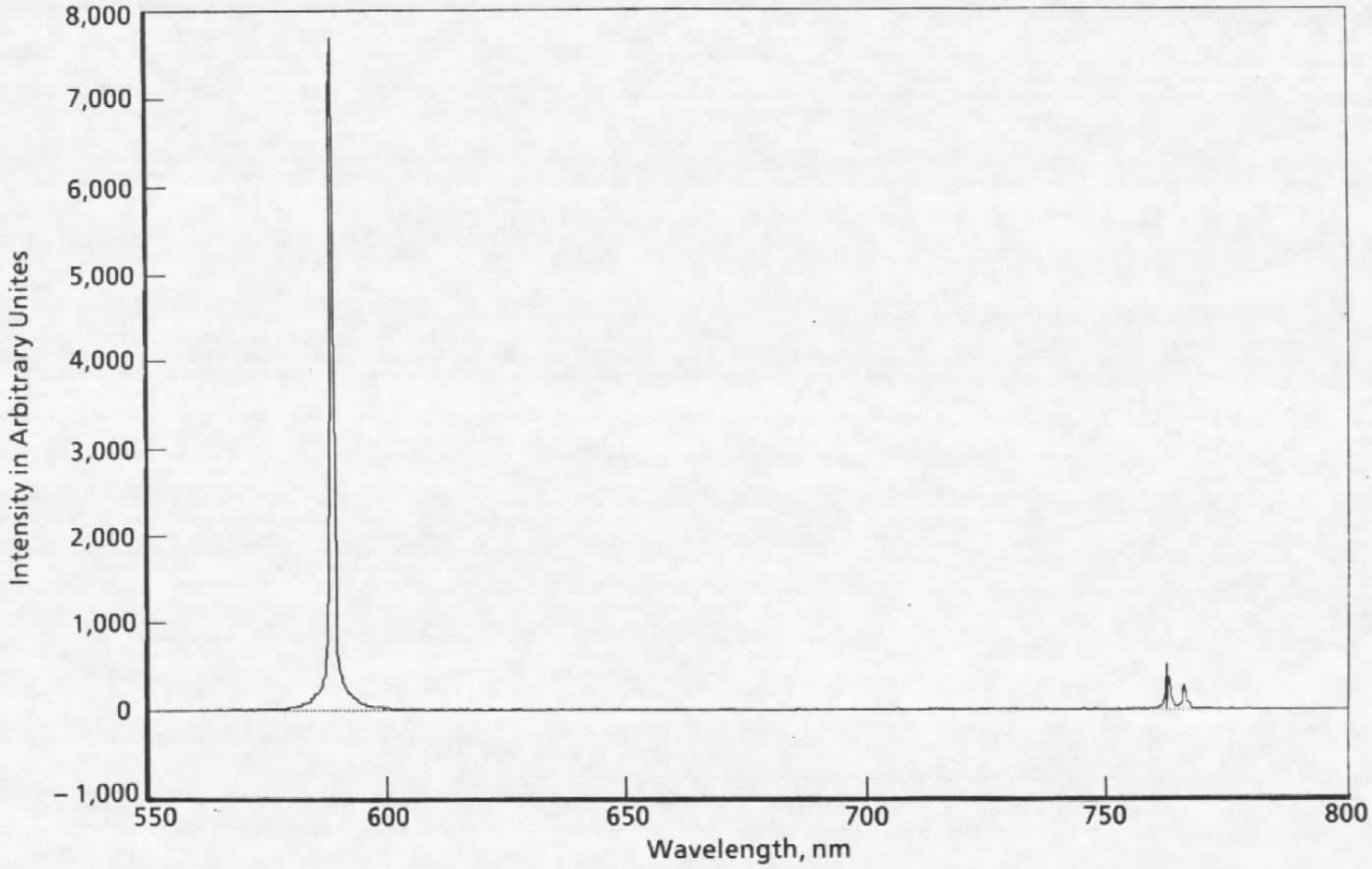

Figure 11. Spectral emission data taken above a stainless steel tube placed in a H_2-air flame.

APPENDIX A

DONNER ALGORITHMS

The Donner algorithms for reconstruction tomography (Ref. 9) are a library of subroutines for three-dimensional reconstruction problems that arise in the medical and physical sciences. These subroutines were written at the Lawrence Berkeley Laboratory of the University of California, Berkeley, CA. They are written in the FORTRAN programming language and are in the public domain. The subroutines have been run at AEDC on the AMDAHL mainframe computer and the IBM RISC 6000 workstation. For industrial computed tomography (CT), the projection data input into the subroutines are normally obtained from transmitted intensity profiles produced as X-rays are transmitted through an object. In addition to transmission data, the medical field also uses emission tomography to determine the concentrations of a radionuclide within the body. As discussed earlier in this report, it is not necessary for the radiation to be X-rays or gamma rays. The mathematics and algorithms apply to visible light as well.

Based on earlier work here at AEDC, three of the nine reconstruction algorithms in the Donner library provided the best reconstructions for our requirements in terms of speed and memory requirements. The classes of algorithms designated as filtered-back projection (the subroutine FILBK) and convolution (subroutine CONVO) are most commonly used in commercial CT systems because of their high speeds. The image quality is excellent if they are given a full complement of input data with high signal-to-noise ratios. The iterative-type algorithms (subroutines CONGR and GRADY) are not used in commercial systems because of their long reconstruction times. When CT data are acquired under dynamic conditions such as rocket motor or turbine engine tests, it is not feasible to acquire a full complement of data, and there is a variety of possible sources of noise. The iterative-type algorithms appear to produce better images from limited data sets; thus, they are used most often at AEDC to reconstruct CT images from test data.

Listed on the following pages is a typical 'main program' used to call a reconstruction routine. The main program allows the user to set the geometry parameters required by the reconstruction subroutine.

Before any of the reconstruction routines are called, the user must call the subroutine SETUP. The arguments of SETUP include control options that describe the geometry as well as some computer operation parameters. In addition, the user must also provide a subroutine GETUM for data input.

MAIN PROGRAM

```
      PARAMETER (NDIMX=180)
      DIMENSION X(NDIMX,NDIMX)
      COMMON /GET/KDUM
      COMMON WORK (300000),ANG(50)
      COMMON/OUTCOM/LUNOUT,I80132
      COMMON/PARM/IPAR(12),PAR(3)
      EQUIVALENCE (NDIMU,IPAR(1)),(ICIR,IPAR(2)),(IGEOM,IPAR(3)),
     1    (NANG,IPAR(4)),(MODANG,IPAR(5)),(KDIMU, IPAR(6)),
     2    (IMIT,IPAR(7)),(NWORK, IPAR(8)),(NFLOAT, IPAR(9)),
     3    (ISTORE,IPAR(10)),(IPRINT,IPAR(11)),(LUNATN,IPAR(12)),
     4    (PWID, PAR(1)),(AXISU, PAR(2)),(RFAN, PAR(3))
      EXTERNAL PRFF,BRFF
      LUNOUT = 6
      I80132 = 1
      NDIMU = 180
      ICIR = 1
      IMIT = 0
      IGEOM = 2
      KDIMU = 235
      NANG = 15
      MODANG = 0
      NWORK = 300000
      LUNATN = 30
      NFLOAT = 1
      ISTORE = 0
      IPRINT = 4
      RFAN = 4367.3364
      PWID = 1.3
      KDUM = KDIMU
      DIMU1 = KDIMU
      AXISU = (DIMU1+1.)/2.
      CALL SETUP(IPAR,PAR,ANG)
      ISTP = 10
      IRLX = 1
      IERR = 0
      IZER = 0
      CALL CONGR(X,PRFF,BRFF,ISTP,IRLX,IERR,IZER)
   22 STOP 23
      END
```

PARAMETER DEFINITION

X	-	THE RECONSTRUCTION ARRAY
PRFF	-	THE PROJECTION SUBROUTINE
BRFF	-	THE BACK-PROJECTION SUBROUTINE
LUNOUT	-	LOGICAL UNIT NUMBER FOR OUTPUT
I80132	-	FLAG INDICATING NUMBER OF CHARACTERS IN A LINE OF OUTPUT ON LUNOUT 0 = 80 CHARACTERS (132 CHARACTERS OTHERWISE)
NDIMU	-	THE LINEAR DIMENSION OF THE RECONSTRUCTION ARRAY
ICIR	-	0 TO RECONSTRUCT A CIRCULAR ARRAY OTHERWISE RECONSTRUCT A SQUARE ARRAY
IMIT	-	0 TO RECONSTRUCT EMISSION DATA OTHERWISE RECONSTRUCT TRANSMISSION DATA
IGEOM	-	GEOMETRY FLAG
0	=	PARALLEL BEAM GEOMETRY
1	=	FAN BEAM GEOMETRY (CURVED DETECTOR)
2	=	FAN BEAM GEOMETRY (FLAT DETECTOR)
3	=	RING DETECTOR GEOMETRY
KDIMU	-	NUMBER OF BINS IN THE PROJECTION ARRAY SUPPLIED BY THE USER
NANG	-	NUMBER OF PROJECTION ANGLES
MODANG	-	MODE FOR PROJECTION ANGLE INPUT
0	=	USER SUPPLIES PROJECTION ANGLES IN DEGREES
1	=	USER SUPPLIES PROJECTION ANGLES IN RADIANS
2	=	PROJECTION ANGLES GENERATED BETWEEN ZERO AND PI STARTING AT THE HALF ANGLE
3	=	PROJECTION ANGLES GENERATED BETWEEN ZERO AND 2*PI STARTING AT THE HALF ANGLE
4	=	PROJECTION ANGLES GENERATED BETWEEN ZERO AND PI STARTING AT ZERO
5	=	PROJECTION ANGLES GENERATED BETWEEN ZERO AND 2*PI STARTING AT ZERO
-I	=	WHERE I IS BETWEEN 2 AND 5 DOES THE SAME AS ABOVE WITH THE ORDER OF ANGLES REVERSED
NWORK	-	DIMENSION OF THE USER'S COMMON BLOCK IN BLANK COMMON
LUNATN	-	LOGICAL UNIT NUMBER FOR ATTENUATION FACTOR STORAGE
NFLOAT	-	NUMBER OF WORDS FOR A FLOATING POINT VARIABLE

ISTORE - 0 TO PERFORM A RECONSTRUCTION OTHERWISE ONLY DO A STORAGE SIZE TEST

WORK - BLANK COMMON WORKING ARRAY

IPRINT - PRINT FLAGS (BIT 0 = LEAST SIGNIFICANT BIT)
BIT 0 PRINT REQUIRED FLOATING POINT BLANK COMMON WHENEVER CHANGED
BIT 1 PRINT PROJECTION DATA AND UNCERTAINTIES
BIT 2 PRINT SETUP VALUES FROM IPAR AND PAR ARRAYS
BIT 3 PRINT FILTER FUNCTION FOR CONVOLUTION AND FILTER ROUTINES
BIT 4 PRINT VALUES FOR THE LAGRANGE MULTIPLIERS AND THE GRADIENT FOR THE FUNCTION OF LAGRANGE MULTIPLIERS FOR THE ENTROPY RECONSTRUCTION
BIT 5 PRINT POINTERS IN BLANK COMMON

RFAN - FOR FAN BEAM GEOMETRY RFAN IS THE DISTANCE FROM THE SOURCE TO THE CENTER OF ROTATION. RFAN IS MEASURED IN UNITS OF PROJECTION BIN WIDTHS AT THE CENTER OF ROTATION.

PWID - PIXEL WIDTH (IN UNITS OF PROJECTION BIN WIDTH)

AXISU - THE PROJECTED LOCATION OF THE ROTATION AXIS IN THE PROJECTION ARRAY (THIS IS SUPPLIED BY THE USER AND IF AXISU IS INTEGER, THEN ROTATION AXIS FALLS IN THE CENTER OF A PROJECTION BIN.)

ISTP - NUMBER OF ITERATION STEPS

IRLX - IRLX IS NON-ZERO FOR ITERATIVE RELAXATION

IERR - IERR IS NON-ZERO FOR WEIGHTED LEAST SQUARE

IZER - IZER IS EQUAL TO 0 IF INITIAL SOLUTION EQUALS 0

IPAR - INTEGER ARRAY WHICH CONTAINS THE OPTIONS AND VARIABLES DESCRIBED IN THE EQUIVALENCE STATEMENT

PAR - REAL ARRAY WHICH CONTAINS THE PARAMETERS DESCRIBED IN THE EQUIVALENCE STATEMENT